AFRL-RX-WP-TP-2008-4019

ESTIMATING THE STRENGTH OF SINGLE-ENDED DISLOCATION SOURCES IN MICRON-SIZED SINGLE CRYSTALS (POSTPRINT)

S.I. Rao, D.M. Dimiduk, M. Tang, T.A. Parthasarathy, M.D. Uchic and C. Woodward

UES, Inc.

OCTOBER 2007

AIR FORCE RESEARCH LABORATORY
MATERIALS AND MANUFACTURING DIRECTORATE
WRIGHT-PATTERSON AIR FORCE BASE, OH 45433-7750
AIR FORCE MATERIEL COMMAND
UNITED STATES AIR FORCE

REPORT DOCUMENTATION PAGE

Form Approved
OMB No. 0704-0188

1. REPORT DATE *(DD-MM-YY)*	2. REPORT TYPE	3. DATES COVERED *(From - To)*
October 2007	Journal Article Postprint	

4. TITLE AND SUBTITLE
ESTIMATING THE STRENGTH OF SINGLE-ENDED DISLOCATION SOURCES IN MICRON-SIZED SINGLE CRYSTALS (POSTPRINT)

5a. CONTRACT NUMBER
FA8650-04-D-5233

5b. GRANT NUMBER

5c. PROGRAM ELEMENT NUMBER
62102F

6. AUTHOR(S)
S.I. Rao and T.A. Parthasarathy (UES, Inc.)
D.M. Dimiduk and M.D. Uchic (AFRL/RXLMD)
C. Woodward (Northwestern University)
M. Tang (Lawrence Livermore National Laboratory)

5d. PROJECT NUMBER
2311

5e. TASK NUMBER
00

5f. WORK UNIT NUMBER
23110002

7. PERFORMING ORGANIZATION NAME(S) AND ADDRESS(ES)

UES, Inc.
4401 Dayton-Xenia Road
Dayton OH 45432-1894

Metals Branch (AFRL/RXLMD)
Ceramics & Nondestructive Evaluation Division
Air Force Research Laboratory
Materials and Manufacturing Directorate
Wright-Patterson Air Force Base, OH 45433-7750
Air Force Materiel Command
United States Air Force

Northwestern University
Department of Materials Science and Engineering
2220 Campus Drive
Evanston, IL 60208-3108

Lawrence Livermore National Laboratory
P.O. Box 808, L-45
Livermore, CA 94551

8. PERFORMING ORGANIZATION REPORT NUMBER

9. SPONSORING/MONITORING AGENCY NAME(S) AND ADDRESS(ES)
Air Force Research Laboratory
Materials and Manufacturing Directorate
Wright-Patterson Air Force Base, OH 45433-7750
Air Force Materiel Command
United States Air Force

10. SPONSORING/MONITORING AGENCY ACRONYM(S)
AFRL/RXLMD

11. SPONSORING/MONITORING AGENCY REPORT NUMBER(S)
AFRL-RX-WP-TP-2008-4019

12. DISTRIBUTION/AVAILABILITY STATEMENT
Approved for public release; distribution unlimited.

13. SUPPLEMENTARY NOTES
Journal article published in Philosophical Magazine, Vol. 87, No. 30, 21 October 2007, 4777–4794. Paper contains color.

14. ABSTRACT
Three-dimensional (3D) discrete dislocation dynamics simulations were used to calculate the effects of anisotropy of dislocation line tension (increasing Poisson's volumes with free surfaces) and to compare them with the strength of double-ended sources of equal length. Their plastic response was directly modeled within a 1 μm^3 volume composed of a single crystal fcc metal. In general, double-ended sources are stronger than single-ended sources of an equal length and exhibit no significant effects from truncating the long-range elastic fields at this scale. The double-ended source strength increases with v, exhibiting an increase of about 50% at v=0.38 (value of Ni) as compared to the value at v=0. Independent of dislocation line direction, for v greater than 0.20, the strengths of single-ended sources depended upon the sense of the stress applied.

15. SUBJECT TERMS

16. SECURITY CLASSIFICATION OF:			17. LIMITATION OF ABSTRACT:	18. NUMBER OF PAGES	19a. NAME OF RESPONSIBLE PERSON (Monitor)
a. REPORT	b. ABSTRACT	c. THIS PAGE			John Barnes
Unclassified	Unclassified	Unclassified	SAR	24	19b. TELEPHONE NUMBER *(Include Area Code)* N/A

Standard Form 298 (Rev. 8-98)
Prescribed by ANSI Std. Z39-18

Philosophical Magazine,
Vol. 87, No. 30, 21 October 2007, 4777–4794

Estimating the strength of single-ended dislocation sources in micron-sized single crystals

S. I. RAO*‡, D. M. DIMIDUK†, M. TANG§,
T. A. PARTHASARATHY‡, M. D. UCHIC† and C. WOODWARD¶

†Air Force Research Laboratory, Materials and Manufacturing Directorate,
AFRL/MLLM Wright-Patterson AFB, OH 45433-7817, USA
‡UES, Inc., 4401 Dayton-Xenia Rd, Dayton, OH 45432-1894, USA
§Lawrence Livermore National Laboratory, P.O. Box 808,
L-45 Livermore, CA 94551, USA
¶Department of Materials Science and Engineering, Northwestern University,
2220 Campus Drive, Evanston, IL 60208-3108, USA

(*Received 4 May 2007; accepted in revised form 23 July 2007*)

Three-dimensional (3D) discrete dislocation dynamics simulations were used to calculate the effects of anisotropy of dislocation line tension (increasing Poisson's ratio, ν) on the strength of single-ended dislocation sources in micron-sized volumes with free surfaces and to compare them with the strength of double-ended sources of equal length. Their plastic response was directly modelled within a $1\,\mu m^3$ volume composed of a single crystal fcc metal. In general, double-ended sources are stronger than single-ended sources of an equal length and exhibit no significant effects from truncating the long-range elastic fields at this scale. The double-ended source strength increases with ν, exhibiting an increase of about 50% at $\nu = 0.38$ (value for Ni) as compared to the value at $\nu = 0$. Independent of dislocation line direction, for ν greater than 0.20, the strengths of single-ended sources depend upon the sense of the stress applied. The value for α in the expression for strength, $\tau = \alpha(L)\mu b/L$ is shown to vary from 0.4 to 0.84 depending on the character of the dislocation and the direction of operation of the source at $\nu = 0.38$ and $L = 933b$. By varying the lengths of the sources from 933 to $233b$, it was shown that the scaling of the strength of single-ended and double-ended sources with their length both follow a $\ln(L/b)/(L/b)$ dependence. Surface image stresses are shown to have little effect on the critical stress of single-ended sources at a length of $\sim 250b$ or greater. This suggests that for 3D discrete dislocation dynamics simulations of the plastic deformation of micron-sized crystals in the size range 0.5–20 μm, image stresses making the surface traction-free can be neglected. The relationship between these findings and a recent statistical model for the hardening of small volumes is discussed.

1. Introduction

Three-dimensional (3D) dislocation dynamics simulations (DDS) have revealed surface-related influences on the motion of dislocations in small simulation cells

*Corresponding author. Email: Satish.Rao@wpafb.af.mil

Philosophical Magazine
ISSN 1478–6435 print/ISSN 1478–6443 online © 2007 Taylor & Francis
http://www.tandf.co.uk/journals
DOI: 10.1080/14786430701591513

designed to represent micron-sized single crystals [1–3]. Recent experimental studies discovered that the proximity of free surfaces bounding small volumes at the micron scale produces strong size-affected strengthening in fcc single crystals, even for high initial dislocation densities [4–11]. In the simulations, the effects arise from the conversion of pre-existing double-ended dislocation sources into single-ended sources that intersect and interact with free surfaces [1, 2]. Such a conversion establishes a new characteristic length for the dislocation sources. The sources in free volumes were shown to adopt configurations that are related to those previously described for small constrained volumes by Blankenhagen *et al.* [12] but with a key difference being that the dislocation lines are truncated by intersecting the free surfaces. In samples below a critical size, the truncation of dislocation sources, together with the under-sampling of an assumed initially random distribution of dislocation sources, leads to smaller average source lengths when compared to a bulk sample of equal dislocation density. This surface-mediated source-hardening contribution was analytically modelled and shown to account for a significant portion of the strengthening experimentally observed in fcc micron-sized crystals [13]. However, for those calculations, the dislocation line tensions were taken to be isotropic and the strength of single-ended dislocation sources of a length L was assumed to be $\alpha\mu b/L$, where α is of the order of 1, μ is the shear modulus and L is the length of the single-ended source [13]. Further, those findings were based upon 3D DDS results that used a simplifying assumption of neglecting image forces for the behaviour of the dislocations that intersected the surfaces of the simulation cell.

In order to lay a foundation for understanding the deformation of freestanding microcolumns, this paper explores the actual source strengths that may be expected for small volumes that contain principally single-armed sources that intersect a surface. Previously, the strengths of single-ended and double-ended sources were modelled using isotropic elastic theory, at a value of Poisson's ratio of 0.333 [14]. These strengths have been evaluated for the special case of a glide plane intersecting the surface at right angles in a semi-infinite-half-space material. As a result, a simple image construction was possible for that analysis to include the influence of image forces on source strength. The study shows that the strengths of single-ended sources are dependent upon the direction of traverse of the source and are weaker than those of double-ended sources by a factor of 1.3–2.6 [14]. The study shows that the scaling of the strength of both single-ended and double-ended sources with their length follows a $\ln(L/b)/(L/b)$ dependence. However, within a current broader context, it is desirable to isolate the influence of the image stress from the overall behaviour of the dislocation sources and to understand the behaviour of such sources for more general dislocation configurations. An added motivation is the significant computational overhead required to accurately account for image forces in a large-scale 3D DDS calculation when that technique is used to represent experimental behaviour. To circumvent that overhead it is highly desirable to employ simpler approximations that are easily implemented in a parallel architecture, while maintaining a reasonable level of accuracy.

Accordingly, in this work a 3D DDS technique is used to calculate the effects of anisotropy of dislocation line tension (within the isotropic elasticity assumption) on the strengths of single-ended sources and to compare them with the strengths

of double-ended sources of equal length. This is done by directly modelling their plastic response within a $1 \times 1 \times 1\,\mu m^3$ volume of fcc Ni single crystal with {001} surfaces, where the glide plane intersects the surface at a crystallographically-appropriate angle of 54.7°. A comparison of simulation results with an accurate consideration of image stresses, here called full free surface treatment (FFST), with similar results that did not include consideration of image stresses, here called simplified surface approximation (SSA), is performed. The FFST and SSA results are in turn compared with the previous findings on strengths of single-ended sources by Pichaud *et al*. [14] and the implications of these results are discussed.

2. Simulation technique

A version of the 3D parallel DDS code ParaDiS [15, 16], developed at Lawrence Livermore National Laboratory, was used to simulate the stress–strain response of single-ended and double-ended sources in a cubic crystal volume with edge lengths equal to 1 μm. In ParaDiS, dislocation lines are represented as a series of nodal points connected by straight-line segments. The glide-plane force on each node is calculated using isotropic linear elasticity and the velocity of a node is taken to be linearly proportional to the force according to a viscous damping law. In these simulations, the velocity was set at a value of $4000b\,s^{-1}$ for a force due to an applied shear stress of 1 Pa, where b is the magnitude of the Burgers vector of the gliding dislocation (0.25 nm). For these simulations the shear modulus and Poisson's ratio were set to values of 59.9 GPa and 0.38, respectively. These values correspond to the shear modulus $= \mu_{111}$ for Ni and Poisson's ratio, $\nu = c_{12}/(c_{11} + c_{12})$, where c_{11} and c_{12} are the cubic single-crystal elastic constants of Ni [17]. To describe anisotropic elasticity effects correctly in the isotropic approximation for double-ended sources, Bacon *et al*. [18] suggest using an isotropic shear modulus as $\mu = 4\pi E_{screw}/b^2$ and, Poisson's ratio, ν, as $1 - E_{screw}/E_{edge}$, where E_{screw} and E_{edge} are the pre-logarithmic line energy factors for infinite straight $a/2\langle 110\rangle$ screw and edge dislocations on the {111} plane in fcc Ni. Such calculations give $\mu = 78.7$ GPa and $\nu = 0.38$ for Ni. Therefore, critical stresses given in this manuscript for single-ended and double-ended sources at a Poisson's ratio of 0.38, must be scaled to a shear modulus of 78.7 GPa from a shear modulus of 59.9 GPa, to obtain their absolute values in Ni.

For these simulations, a constant strain rate of $50\,s^{-1}$ was imposed along the $[41\bar{3}]$ crystal direction. The $(1\bar{1}\bar{1})[110]$ slip system is maximally stressed under these conditions, having a Schmidt factor of 0.47. Both the single-ended and double-ended sources in the simulation were operative on this slip system. If at any time step, the specimen plastic displacement rate was lower than the applied rate, the applied stress was incremented to obey a constant applied displacement rate, i.e. for $d\varepsilon_p/dt < d\varepsilon/dt$, $d\varepsilon_p/dt + d\varepsilon_e/dt = d\varepsilon/dt$, where ε_p, ε_e and ε are the plastic, elastic and total strains, respectively. However, if the specimen plastic displacement rate was higher than that of the programmed rate, the applied stress was kept constant, thus permitting source expansion i.e. for $d\varepsilon_p/dt > d\varepsilon/dt$, $d\sigma = 0$. Once the $d\sigma = 0$ condition was satisfied, increments in stress occurred only after it was determined that the total displacement

at a particular time was less than the applied displacement rate multiplied by the elapsed time, i.e $\varepsilon_p + \varepsilon_e < d\varepsilon/dt(\Delta t)$.

The ParaDiS code was modified in the following manner to qualitatively account for dislocation surface effects (the SSA). This approximation to the dislocation–surface interaction is similar to the ones previously used in the literature for 3D dislocation dynamics simulations of confined systems [19–21]. As dislocation segments expand they eventually reach the surface, and those that lay on the surface are deleted as though they exited the glide plane of the dislocation source. Further, within the SSA method, the velocity of the terminal dislocation node at the surfaces (surface nodes) is modified such that the velocity components perpendicular to both the free surface and the glide plane were zero, causing the node to track the surface trace of the slip plane. As described in section 4 we found that the SSA treatment, not only qualitatively captures the most important free surface effect of establishing a new critical source length for flow, but is also computationally efficient within a parallel environment. Separate simulations using a serial version of ParaDiS were used to show that small changes in the strength of single armed sources can be expected due to the influence of the image forces acting on dislocations from free surfaces (our FFST method). Selected source configurations acting under the influence of image forces were examined to quantify these effects. The image stresses were modelled using a hybrid technique where the singular and non-singular parts of the image stresses are dealt with separately [22]. The analytic solution for a semi-infinite straight dislocation intersecting the surface of elastic half-space is used to account for the singular part of the image stress, while the remaining non-singular part is treated using the standard finite-element method [22].

3. Sources within the simplified surface approximation

One objective for this work was to determine the effect of the line energy anisotropy on the strength of single-ended and double-ended dislocation sources in small material volumes. Consequently, four types of simulations were conducted: (i) double-ended sources for both isotropic and anisotropic line energies; (ii) single-ended sources for both isotropic and anisotropic line energies; (iii) single-ended sources of varying line orientation with anisotropic line energy; and, finally, (iv) single-ended and double-ended sources of varying line length with anisotropic line energy. For the first case, analytical results exist in the literature for an equivalent configuration acting within an infinite volume and these are used for comparison. In the isotropic limit, the strength of a single-armed source is expected to be half that of a double-ended source of the same length. These prior results were verified for a small volume and then the effects of dislocation line energy anisotropy and line character on both double-ended and single-ended sources were examined. Three dislocation characters, edge, screw and 30° mixed dislocation characters were considered.

3.1. *Double-ended sources in a small volume*

The source strengths for double-ended sources in small crystals were calculated using sources of length 933b, approximately one-fourth the cube edge length, placed at the centre of a cube of material, the sides of which were 1 μm in length. Note that for this source geometry, the double-ended source achieved its critical configuration without intersecting the free-surface. The effect of Poisson's ratio was calculated using a 30° mixed-character dislocation and the results are shown in figure 1. For the double-ended sources in an infinite medium, the critical stress as a function of Poisson's ratio can be written as [18]

$$\tau(\upsilon) = \frac{\alpha\mu b}{L} = \frac{\mu b}{L} C\left(\frac{3}{4(1-\upsilon)} + \frac{1}{4}\right). \tag{1}$$

A fit of equation (1) to the simulated critical stress data for double-ended sources is shown in figure 1 and the correspondence is very good for a value of $C = 0.823$. Thus, the influence of the finite volume is negligible for double-ended sources that are completely contained within the boundaries of the crystal at the 1 μm scale and above. This is due to the fact that the Frank–Read source was placed exactly at the centre of the 1 μm cubic simulation cell, where the image stresses from opposite free surfaces exactly cancel each other. In general, image stresses near a single free surface is approximately equal to $\mu b/4\pi l$, where l is the distance from the surface to the source [23]. The stress to operate a Frank–Read source of length L is

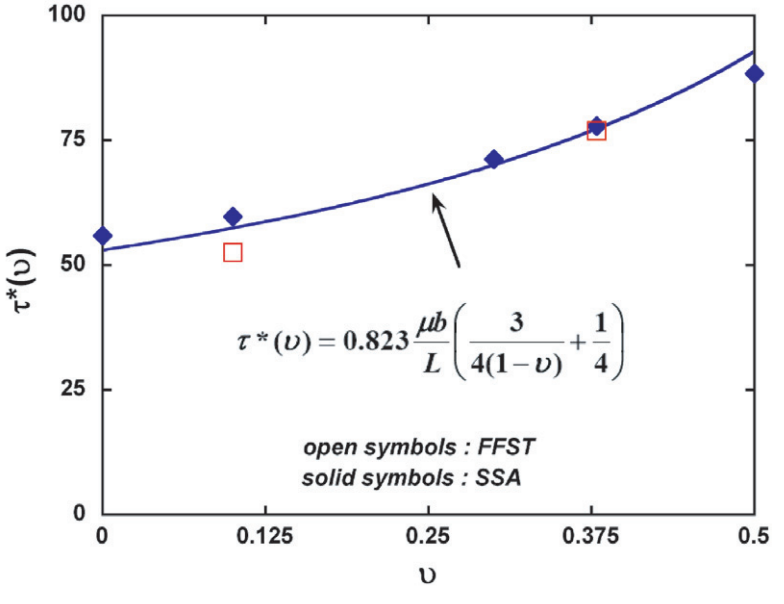

Figure 1. The critical resolved shear stress, $\tau^*(\upsilon)$, for a double-ended source having 30° mixed dislocation character as a function of Poisson's ratio. Critical stresses are in MPa. The line gives the best fit of the simulation-based empirical relation given by Bacon *et al.* [18] for infinite crystals, with C = 0.823. Results from FFST method are denoted by open symbols.

approximately equal to $\mu b/L$. Therefore, image stresses will have a significant effect on the Frank–Read source operation stress only when L is of the order of $4\pi l$ and the Frank–Read source is approximately parallel to the free surface.

3.2. *Single-ended sources in a small volume*

Critical stresses were evaluated for the single-ended sources as a function of Poisson's ratio, keeping the source length constant at $933b$. The results are shown in figure 2 for the case of a source the initial configuration of which was a straight line extending from a fixed node inside the cube to the surface and the line character being a 30° mixed dislocation. The strength of this source depended upon both the sign of the applied stress that resulted in the 'forward' or 'reverse' operation of the source, and the degree of line anisotropy. The results are shown in comparison to a double-ended source, which has the same critical stress for both forward and reverse operation. As shown in figure 2, it can be seen that for the case of isotropic line tension ($\nu = 0$–0.1), the source strength of a single-armed dislocation source is nearly half that of the equivalent length double-ended source. This result is in agreement with published estimates of the critical stress for single-ended sources in a line energy isotropic material [23]. In addition, there is no significant difference between the forward and reverse directions for the isotropic line tension case.

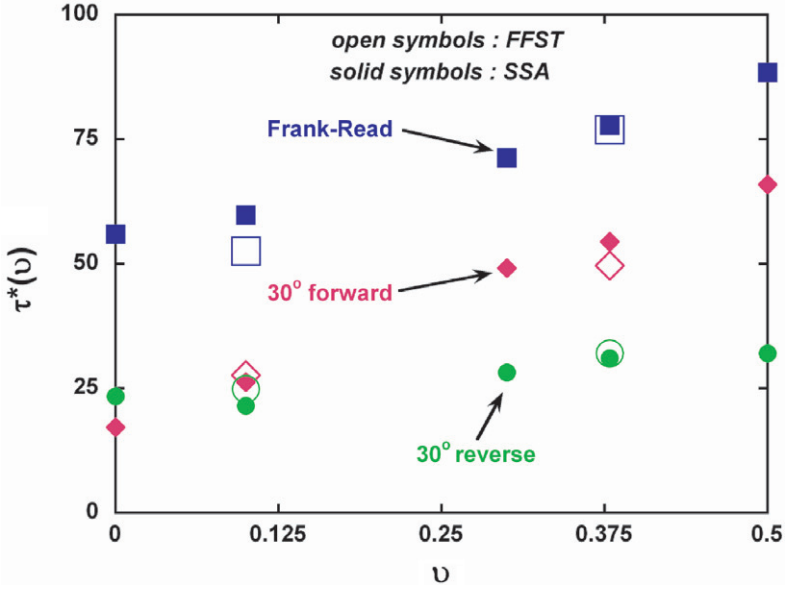

Figure 2. The critical resolved shear stress, $\tau^*(\nu)$, for a single-ended source of 30° mixed character compared with the result for a double-ended source of the same length. Critical stresses are in MPa. Unlike the double-ended source, the single-ended source has a different critical stress depending upon the forward or backward direction of operation. Results from FFST method are denoted by open symbols.

However, for the anisotropic line energy case ($\nu > 0$), figure 2 shows that for the forward direction, the critical stresses increase rapidly with increasing Poisson's ratio (similar to those for double-ended sources). However, for the reverse direction, the source strengths increase more gradually. When ν is large (>0.3), the critical stresses for single-ended sources are more than half of those for double-ended sources when stresses act in the forward direction, and less than half when stresses act in the reverse direction. These results are similar to the simulation results of Pichaud *et al.* [14], who considered the case of a Poisson's ratio of 0.333. Note that for all of the fcc microcrystals used in experimental studies reported in the literature, i.e. Cu, Ni, Au and Al [4–11], ν is relatively large (>0.3) and the anisotropy in critical stress between the forward and reverse directions for the 30° single-ended source is expected to occur. This result suggests that there is an intrinsic scatter to the source strengths even for fixed source lengths.

3.3. *Origin of source strength asymmetry*

For the small volumes examined here, the stress–strain curves and dislocation configurations at the critical stress offer insights into the nature of the source-strength asymmetry with respect to the direction of operation. Consider a single-ended source of length $933b$, inserted into a $4000b$ cubic simulation cell ($\nu = 0.38$), residing on a $(1\bar{1}1)$ plane and having its fixed point inside the cell and the other end on the (100) surface. For the 30° mixed-character dislocation line source, this source has a line direction [211], which is 30° away from the [110] screw-line direction and perpendicular to the surface edge trace, a $[01\bar{1}]$ direction. Figure 3 shows the stress–strain response of the forward and reverse operation of such a source along with a pure screw character single-ended source. The stress–strain response of the forward operating 30° source was purely elastic-plastic with a critical stress of 114 MPa (CRSS of 54.5 MPa in figure 2). At the critical stress, the single ended-source completely traverses the $(1\bar{1}\bar{1})$ glide plane leading to uncontrolled plastic deformation of the microcrystal volume. The stress–strain response of the screw-character source was qualitatively similar to the forward operating source save for a critical stress of 90 MPa (CRSS of 42.3 MPa in figure 2). In this case, the Burgers vector of the initial source with a magnitude of $a/\sqrt{2}$ was chosen, for convenience, to be a [211] direction such that the initial source had a screw-character direction. For the 30° reverse source, the sign of the input Burgers vector was reversed as compared to 30° forward source, such that the source moves in the opposite direction under the same applied stress. Unlike the other two single-ended sources, the stress–strain curve shows a small strain burst at 57 MPa (CRSS of 27.2 MPa in figure 2) before uninhibited plastic deformation at 64 MPa (CRSS of 30.6 MPa in figure 2).

Figure 4 shows the initial (stress free) and critical configuration (maximum stress) of these sources. The results show that at the very beginning of the simulation, when the applied stress is almost zero, both 30° sources rotate from their initial line direction to the screw-character position, a ⟨110⟩ direction. This occurs because of the lower line-energy per-unit-length for the screw-character dislocation. It is known in the literature that the most frequently observed surface effect for dislocations

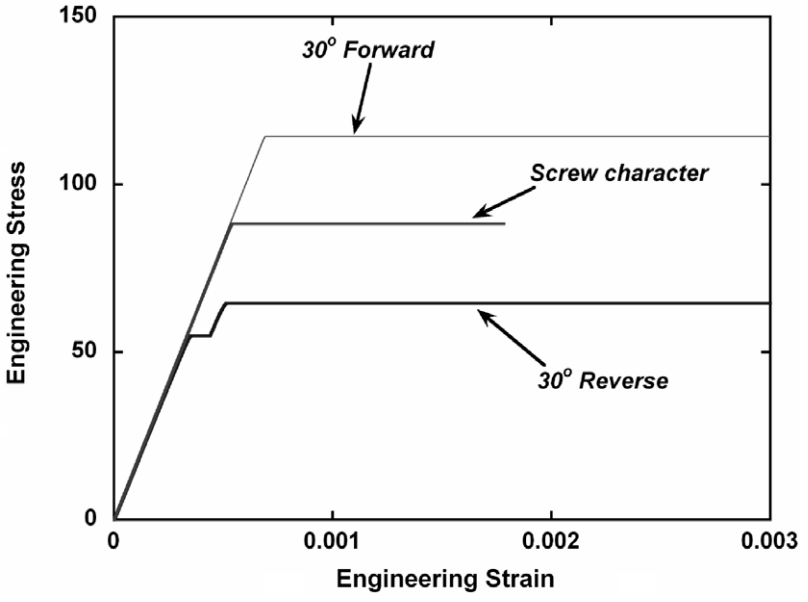

Figure 3. Stress–strain curves for three single-ended sources of length 933*b*, 30° forward, 30° reverse and screw character in a 1 μm cubic cell using the SSA method. Stresses are in MPa. Shear modulus = 59.9 GPa and Poisson's ratio = 0.38. The cubic cell was stressed in the $[41\bar{3}]$ direction.

is Lothe's force which causes dislocations to rotate to lower their line energy [24]. Thus, the energy increase due to the necessary line length increase as it rotates is more than offset by the energy decrease due to line direction change, from 30° to 0°. It is noted, however, that the amount of this rotation is not in agreement with Lothe's formula [24], since without image stresses, force equilibrium is not achieved on the surface. For the screw-character source case, no rotation needs to occur since the initial line direction is the low-energy configuration. The critical configurations for these sources are shown in figure 4. The line tension forces tend to curve the sources about the fixed point and the screw-character direction. Upon application of the applied stress, the direction of traverse for the single-ended source acting in the 30° forward case is such that the source initially decreases its line length. However, for the 30° reverse source, the source is moving in a direction that continually increases line length as it travels toward the critical configuration. Therefore, the asymmetry in the critical stress between the 30° forward and reverse directions of motion is most probably related to line tension forces. These forces make it easier for the source to curve in a direction with increasing line length as compared to a direction with decreasing line length. For the screw-character case, the source is curving about the fixed point and the initial direction, which has a line length intermediate to the previous two cases and, the corresponding critical stress of 90 MPa lies between 114 MPa (30° forward) and 57 MPa (30° reverse). For both the 30° forward and screw-character cases, once the source overcomes the critical configuration, it continuously traverses the glide plane leading to uninhibited

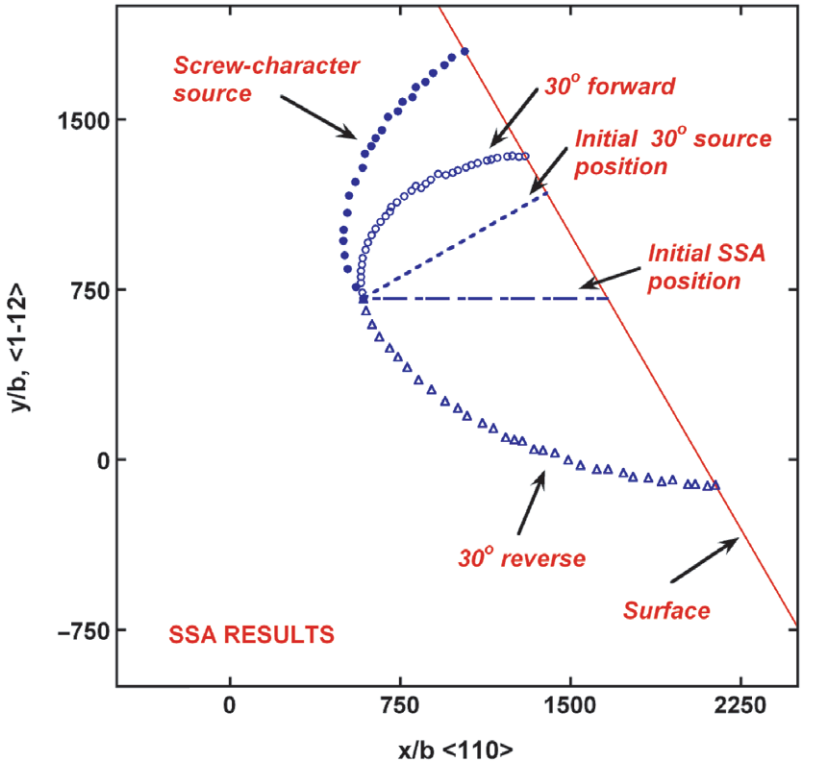

Figure 4. Critical configurations of a 30° single-ended source moving in forward and reverse directions and a screw-character source of length 933b in a 1 μm cubic cell. Shear modulus is 59.9 GPa and Poisson's ratio = 0.38. The initial rotation of the 30° source is also depicted. All results are for the SSA method.

plastic deformation. For the 30° reverse case, once the source overcomes the critical configuration shown in figure 4 (small strain burst in figure 3), it traverses the glide plane and reaches another critical configuration on the opposite surface edge, which corresponds (in our nomenclature) to a 30° forward source for the opposite surface edge, with a larger length. The second critical position is overcome at a stress of 64 MPa and, thereafter, the source continuously traverses the glide plane.

These results suggest that for $\nu = 0.38$ (i.e. pure Ni), the 30° single-ended source has strengths of approximately $0.8\,\mu b/L$ in the forward direction and $0.4\,\mu b/L$ in the reverse direction, whereas double-ended sources are stronger than the corresponding single-ended sources.

4. Effect of image stresses using the full free surface treatment

In the previous section, calculations of the plastic response of single-ended sources of length 933b in a 1 μm cubic cell were presented. For those simulations the image stresses that make the surface traction-free were not considered. For the set of

simulations presented in this section, the images forces were included by the following method. A different serial version of the ParaDiS code with a hybrid technique [22] for calculating the image stresses was employed. The hybrid technique considers the image-stress field as a superposition of analytic and FEM based solutions. The analytic solution is the image-stress field of a semi-infinite straight dislocation intersecting the free surface of a semi-infinite half-space. The geometry of this dislocation is chosen such that its image stress contains the same singularity as the image stress of the dislocation of interest. The second, FEM solution, is the difference between these two image stress fields and by construction it is a non-singular function of space and converges much faster than a direct FEM calculation of the complete image-stress field [22, 25].

When image stresses are also considered for the simulation cell, there are minor differences in the exact configurations and critical stresses adopted by dislocation sources. For example, the 30° single-ended source does not rotate all the way to the screw-character line position as was seen in the earlier SSA-method calculations. Rather, that source rotates to a position 10–15° away from the screw-character position (see figure 5). With image forces imposed, the source tries to lie orthogonal

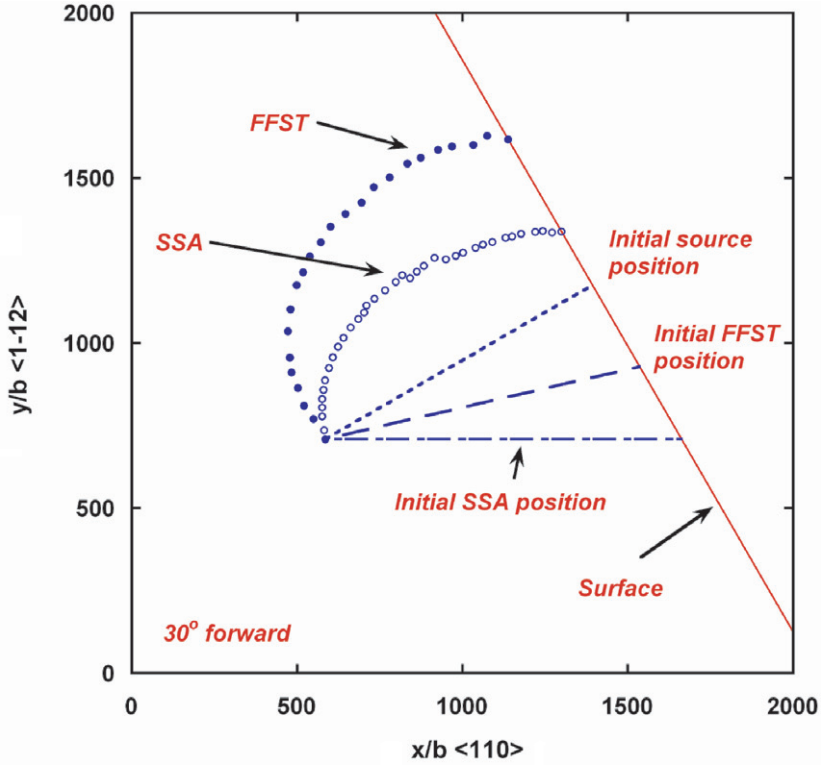

Figure 5. Comparison of the critical configurations of a 30° single-ended source moving in the forward direction with and without image stresses (both SSA and FFST methods). Shear modulus is 59.9 GPa and Poisson's ratio = 0.38. The initial rotation of the source is also depicted.

to the cell surface [14], but these forces are resisted by line tension forces that push the line towards the screw-character position. Thus, the balancing of these two forces results in an initial position which is in between the initial 30° position and the screw-character position and thereby a slightly altered source length. The amount of this rotation is in agreement with Lothe's formula [24]. Also, image stresses are expected to be identically equal to zero all along the source at this initial rotated position [21], leading to no curvature of the source at this initial position. Under continued increase in stress, the source then bows around this initial configuration and the fixed point to attain the critical configuration at a stress of 104 MPa (CRSS of 49.7 MPa in figure 2). The final distance to the surface at the critical configuration is slightly larger as compared to the SSA-method case, resulting in a slight decrease of the critical stress (~10%). For the 30° reverse case, the critical stress with the FFST is slightly larger, 60 MPa (CRSS of 28.7 MPa in figure 2), as compared to the results from the SSA method. In this case, the stress increases as a result of both the image and line energy forces tended to work against the applied stress, thus reducing the source length relative to the image-free source.

Figure 6 shows the critical stresses using the FFST method for the 30° forward and 30° reverse cases, which are similar to the results shown in figure 2. A direct comparison of the source critical stresses between these two figures reveals that within the present image-force analysis there is only a modest effect when image stresses are included. Overall, image stresses have only a slight effect (<~10%) on the critical stresses of single-ended sources at these sizes.

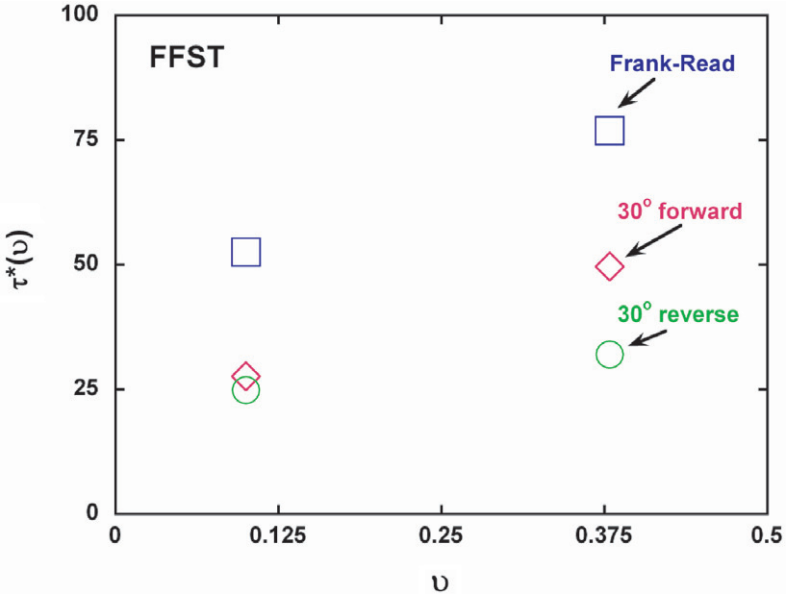

Figure 6. Critical resolved shear stresses, $\tau^*(\nu)$, for single- and double-ended (Frank–Read) sources of 30° mixed character and length 933*b*. Results shown are for $\nu = 0.1$ and 0.38. Image stresses are included in the simulations using the FFST method. Critical stresses are in MPa.

Prior studies of image-force effects reported in the literature [24] suggest that image stresses decrease rapidly as one moves away from the free surface, taking on a value of only about 10 MPa for distance of about 50–100b away from the free surface. This distance is equivalent to one or two nodes at or near the surface for the discretization lengths typically used in the present (and other) DDS simulations. Since the source length considered here is an order of magnitude larger than this image-stress decay distance, it is not surprising that image stresses have little effect on the critical stress of single-ended sources of length 933b. They are expected to become more significant as the source length is decreased below ~250b. In spite of these results showing a negligible influence of the image stresses, it is important to note an alternate effect that was not investigated in the present study. From prior studies, image stresses are also known to significantly increase the propensity for screw-character dislocations to cross-slip near surfaces. This occurs by the image forces acting to constrict the Shockley partials of the $a/2\langle 110\rangle$ screw-character dislocation at some surfaces [24, 26, 27]. Dislocation cross-slip has not been considered in the simulation results presented here. Any cross-slip at or near the surface due to image stresses may result in a complete or partial pinning of the dislocation at the point of surface intersection, even if for no other reason than a lowering of resolved stress on the cross-slipped segment relative to the primary internally-pinned segment, thus raising the strengths of single-ended sources towards those of a double-ended source of the same length. Thus, the present results from both the SSA and FFST methods must be viewed only as plausible lower bounds on single-ended source strengths.

5. Length scaling of the critical stress of single-ended and double-ended sources

Figure 7 shows a plot of the critical resolved shear stress of double-ended (30°) and single-ended (30° forward and 30° backward) sources, as a function of source length varying from 233 to 933b, at $\nu = 0.38$. Also shown in the plot are fits to the simulation data using an equation of the form

$$\tau(L) = k\mu \frac{\ln(L/b)}{(L/b)}, \tag{2}$$

where k is a constant. It is seen that equation (2) fits the simulation data well, with k being 0.06 for single-ended sources (backward), 0.12 for single-ended sources (forward) and 0.18 for double-ended sources. From prior literature reports, it is known that the critical stresses of double-ended sources scale according to equation (2) [28, 29].

Figure 7 shows that scaling according to equation (2) is also valid for single-ended sources, as was observed in the simulations of Pichaud *et al.* [14] for lengths in the range 10^3–$10^6 b$. Also, note that the simulations leading to figure 7 were performed using the SSA method. As discussed previously, image stresses are expected to influence the strength of single-ended sources only when the lengths of the sources reach ~250b or less. Therefore, equation (2) can be considered valid

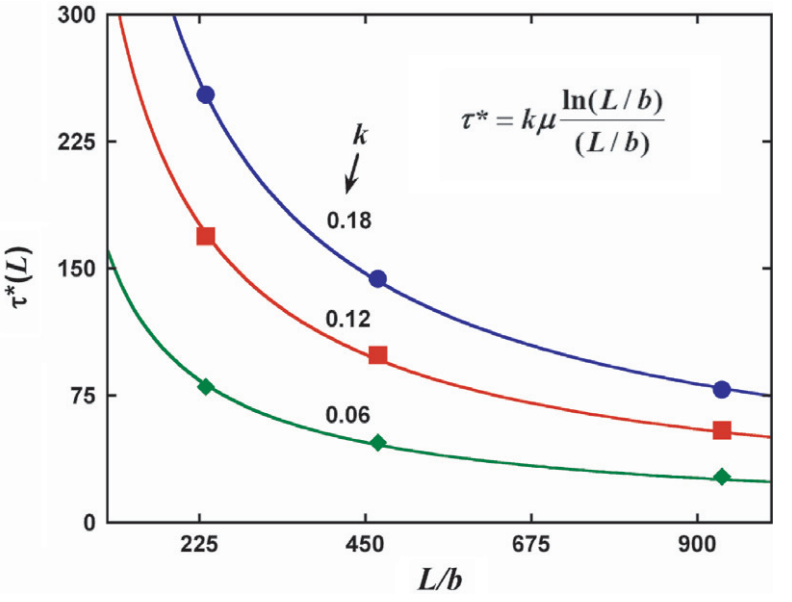

Figure 7. Critical resolved shear stress (τ^*) of 30° single- and double-ended (Frank–Read) sources as a function of length L of the sources. Also shown are $k\mu\ln(L/b)/(L/b)$ fits to the simulation data (solid lines). $k = 0.06$ (single-ended backward); $k = 0.12$ (single-ended forward) and $k = 0.18$ (double ended). All results are for the SSA method. Critical stresses are in MPa.

for single-ended sources, for source lengths greater than $500b$, as used for analysis of the Ni microcrystals [13]. Pichaud *et al.* [14] give an equation for k for single-ended sources, for a Poisson's ratio of 0.333 and the special case of a glide plane intersecting the free surface at right angles as

$$k = 0.108 + 0.040\cos(2\phi + \pi/3), \tag{3}$$

where ϕ is the angle between the Burger's vector and line direction of the single-ended source. Our results for 30° (forward and reverse) as well as screw sources, at a Poisson's ratio of 0.38 and wherein the glide planes intersects the free surface at a crystallographically appropriate angle of 54°, is within 15% of equation (3).

For dislocation sources, the balance between dislocation line length and line curvature leads to the following expression for the critical resolved shear stress versus source length:

$$\tau(L) = \frac{\alpha\mu b}{L}, \tag{4}$$

where L is the length of the single-ended or double-ended source. The parameter α is the source-strength coefficient that varies with the exact nature of the source, length of the source and the material. For these simulations, the value of Poisson's ratio was fixed at 0.38 and the values for α were determined at a length of $933b$. Table 1 shows values for the coefficient for various sources that indicate a variation from 0.4–0.84 for single-ended sources and, 0.8–1.28 for double-ended sources in

Table 1. Measure of strength of single-ended and Frank–Read sources, α, at a Poisson's ratio, ν, of 0.38 and length of 933b.

Source	α (using SSA)
Single-ended (30° forward)	0.84
Single-ended (30° reverse)	0.4
Single-ended (screw)	0.66
Frank–Read (screw)	1.28
Frank–Read (30°)	1.19
Frank–Read (edge)	0.86

small volumes. Clearly, the double-ended sources are stronger than the single-ended sources of the same length. The coefficient α at any length of the single-ended or double-ended sources can be obtained from their corresponding value at 933b as

$$\alpha(L) = \alpha_{933b} \frac{\ln(L/b)}{6.84}. \tag{5}$$

6. Discussion and summary

The results of this study can be summarized as follows.

1. The strengths of single- and double-ended dislocation sources were determined for a 4000b cubic simulation cell using a 3D DDS code and a simplified treatment of surface conditions that is amenable to efficient parallel computing. The initial length of the sources was fixed at 933b for this cell and both the line energy anisotropy (Poisson's ratio) and line character were varied.
2. Single-ended sources are weaker than the corresponding full Frank–Read sources, with the measure of strength α for single ended sources varying between 0.4–0.84 and, for double ended sources varying between 0.86–1.28, at a Poisson's ratio of 0.38. There was no observable influence from truncating an infinite volume at the 1 μm scale for the double-ended sources. In general, image stresses are expected to influence the double-ended source operation stress only when their length L is of the order of or greater than $4\pi l$, where l is the distance to the surface from the source.
3. There is an asymmetry in the strength of single-ended sources depending upon the direction of traverse of the source. The direction where the source length initially decreases is stronger for Poisson's-ratio values greater than 0.2. This is in agreement with previous results from Pichaud *et al.* [14] on the strength of single-ended sources for the special case of a glide plane intersecting the surface at right angles and a Poisson's ratio of 0.333.
4. For a separate set of simulations the near-surface image force was introduced and its influence on source strength was examined for a source length of 933b to check the effect of the SSA. At these source lengths, image stresses have a small effect (<10%) on the strength of single-ended sources.

5. In the absence of image stresses, the scaling of the strength of single-ended and double-ended sources with their length follows a $\ln(L/b)/(L/b)$ dependence. This is in agreement with previous results from Pichaud *et al.* [14] for source lengths ranging from 10^3b to 10^6b.
6. Comparison of the present results on the strength of single-ended sources with previous results from Pichaud *et al.* [14] suggests that the strength of single-ended sources follows equation (2) with k given by equation (3) (within 15%) [13], for source lengths greater than $500b$.

The single-ended sources envisaged here for micron-sized crystals are conceptually similar to the ones proposed by Blanckenhagen *et al.* [12] for the strengthening of constrained micron-scale volumes. Both concepts involve the setting of a new dislocation source length that is different from the initial source and governed by the presence of a constraining surface. However, there are significant quantitative differences between the constraints imposed by a grain boundary wherein the full dislocation loop is envisaged to be retained (such as in the work by Blankenhagen *et al.* [12]), and those imposed at a free surface where the loop shape is lost and the dislocation may be free to move under a more gentle curvature. In the Blanckenhagen *et al.* [12] model, the impenetrable grain boundary sets a new smaller length for the operation of the Frank–Read source, for initial Frank–Read source sizes that are larger than 1/3 the grain diameter. Thus, strengthening of the system occurs as the result of a constrained smaller source length. Herein, single-ended sources form with the dislocation being mobile on the free surface and thus are weaker than the corresponding Frank–Read sources of an equal length in the bulk. However, other simulations suggest that microcrystals that form such configurations are strengthened nonetheless [1, 2, 13]. They are strengthened because of reduced number of available longer-length mobile segments once surface interactions become important. The internal pinning points that form these sources are thought to originate from jogs coalescing into superjogs within the grown-in dislocation network and/or by double cross-slip of screw-oriented segments [30].

These findings reinforce the statistical model suggested by Parthasarathy *et al.* [13] which used source-strength coefficients that are generally of the order of those calculated in this work. Thus, it is readily expected that the single-ended sources can result in hardening a small deforming volume provided that the stochastic aspects of that model are representative of physical microcrystals. This is illustrated by figure 8 (adapted from Parthasarathy *et al.* [13]) wherein the average length of single-ended sources, scaled by the diameter of the simulation cell, is plotted against the number of initial mobile sources in the sample, again for a fixed starting dislocation density. Also shown in figure 8 is the standard deviation in the source lengths as a function of number of initial mobile sources in the sample. Figure 8 clearly shows that as the number of initial mobile sources decreases, the average source length scaled to the diameter decreases significantly. As the number of initial mobile sources decreases (decreasing sample size), the strengths of single-ended sources becomes important, even though they are weaker than equivalent-length double-ended sources. Thus, for small micron-scale volumes, single-ended sources are expected to control plastic deformation and to lead to high initial stresses in micrometer-sized volumes [13].

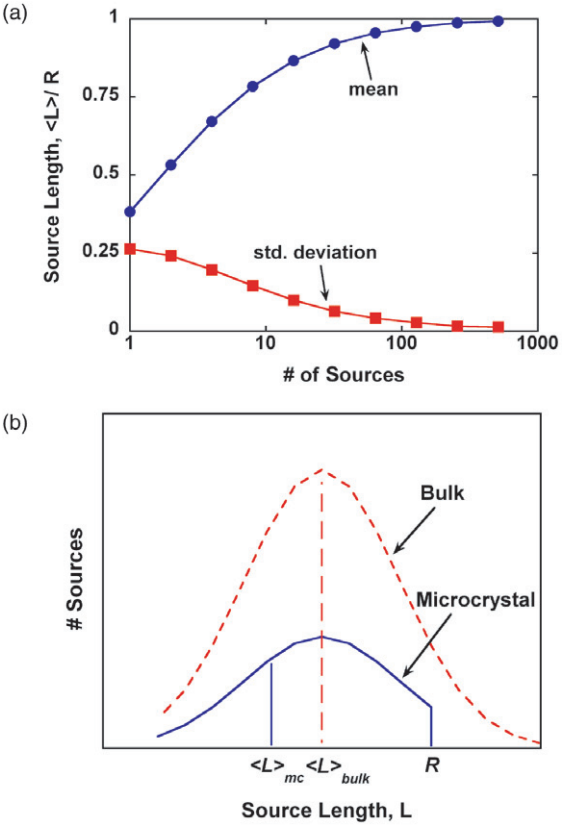

Figure 8. (a) Average source length, $\langle L \rangle$ (scaled to the radius of the sample, R) versus the number of initial mobile sources in the sample (based on an initial dislocation density [11]). (b) Schematic illustration of source length probability distributions for microcrystals versus bulk samples following model developed by Dimiduk *et al.* [11].

In the statistical model of Parthasarathy *et al.* [13], the strength of single-ended sources was taken to be approximately equal to $\langle \alpha \rangle \mu b/L$, where $\langle \alpha \rangle$ was taken to be 1. The range of sample diameters considered in the model was 1–20 μm and the sample radius was chosen as the maximum source length, L. From that statistical analysis, the average length of single-ended sources, over that range of sample diameters, is a factor of 5–10 larger than the value of $933b$ selected in this study. The simulations presented here give α in the range of 0.54 to 1.12 at a length of $9330b$ for single-ended sources and the SSA [equation (4)], with an average value of 0.83. Therefore, the value of 1 chosen for $\langle \alpha \rangle$ previously [13] is a slight overestimate of the contribution of source-truncation hardening to the strengthening observed at small sizes in microcrystal experiments [4–11].

However, 3D dislocation dynamics studies [1] also show that in addition to source-truncation hardening another mechanism of strengthening is present in micron-sized crystals, 'exhaustion hardening', which is related to the cessation of initially-operating single-ended sources due to interaction with obstacles and the

reactivation of these original sources or activation of new sources at larger stresses. This second mechanism of strengthening has not been taken into account in the statistical model and could account for discrepancy between the experimental strengthening data and the statistical model of Parthasarathy *et al.* [13].

Acknowledgements

The authors acknowledge use of the 3D DDS code, ParaDiS, which was developed at Lawrence Livermore National Laboratory by the ParaDiS team. The work of M. Tang is performed under the auspices of the United States Department of Energy by the University of California. This work was supported by the AFOSR, and by a grant of computer time from the DOD High Performance Computing Modernization Program, at the Aeronautical Systems Center/Major Shared Resource Center. The work was performed at the US Air Force Research Laboratory, Materials and Manufacturing Directorate, Wright-Patterson AFB.

References

[1] S.I. Rao, T.A. Parthasarathy, M. Tang, *et al.*, paper presented at the 3rd International MMM Conference, Freiburg, 18–22 September (2006).
[2] H. Tang, K.W. Schwarz and H.D. Espinosa, Acta mater. **55** 1607 (2007).
[3] D. Weygand, M. Poignant, P. Gumbsch, *et al.*, Mater. Sci Engng A (in press).
[4] M.D. Uchic, D.M. Dimiduk, J.N. Florando, *et al.*, Mater. Res. Soc. Symp. Proc. **753** 27 (2003).
[5] M.D. Uchic and D.M. Dimiduk, Mater. Sci. Engng A **400–401** 268 (2005).
[6] D.M. Dimiduk, M.D. Uchic and T.A. Parthasarathy, Acta Mater. **53** 4065 (2005).
[7] D.M. Dimiduk, C. Woodward, R. LeSar, *et al.*, Science **312** 1188 (2006).
[8] M.D. Uchic, D.M. Dimiduk, J.N. Florando, *et al.*, Science **305** 986 (2004).
[9] J.R. Greer, W.C. Oliver and W.D. Nix, Acta Mater. **53** 1821, errata (2005).
[10] C.A. Volkert and E. Lilliodden, Phil. Mag. **86** 5567 (2006).
[11] D.M. Dimiduk, M.D. Uchic, S.I. Rao, *et al.*, Modell. Simul. Mater. Sci. Engng **15** 135 (2007).
[12] B.V. Blankenhagen, P. Gumbsch and E. Arzt, Phil. Mag. Lett. **83** 1 (2003).
[13] T.A. Parthasarathy, S.I. Rao, D.M. Dimiduk, *et al.*, Scripta. Mater. **56** 313 (2007).
[14] B. Pichaud, F. Minari and J. Kellerhals, Phil. Mag. A **38** 593 (1978).
[15] W. Cai, V. Bulatov, T. Pierce, *et al.*, Solid Mech. Appl. **115** 1 (2004).
[16] A. Arsenlis, W. Cai, M. Tang, *et al.*, Modell. Simul. Mater. Sci. Engng, accepted (2007).
[17] A.J. Ardell, Metall. Trans. A **16** 2131 (1985).
[18] D. Bacon, D. Barnett and R. Scattergood, Prog. Mater. Sci. **23** 51 (1980).
[19] B. Devincre, in *Computer Simulation in Materials Science*, edited by H.O. Kirchner, V. Pontikis and L.P. Kubin (Kluwer Academic, Dordrecht, The Netherlands, 1996).
[20] K. Schwarz, J. Appl. Phys. **85** 108 (1999).
[21] X.H. Liu and K. Schwarz, Modell. Simul. Mater. Sci. Engng **13** 1233 (2005).
[22] M. Tang, W. Cai, G. Xu, *et al.*, Modell. Simul. Mater. Sci. Engng **14** 1139 (2006).

[23] J.P. Hirth and J. Lothe, *Theory of Dislocations*, 2nd ed. (John Wiley and Sons, New York, 1982).
[24] P.M. Hazzledine, in *Fundamentals of Deformation and Fracture*, edited by B.A. Bilby, *et al*. (Cambridge University Press, Cambridge, 1985).
[25] M. Tang, G. Xu, W. Cai, *et al*., in *Thin Film Stresses and Mechanical Properties*, edited by S.G. Corocoran, Y.-C. Joo, R.N. Moody and Z. Zuo (Materials Research Society, Warrendale, PA, 2003).
[26] P.M. Hazzledine and S.J. Shaibani, in *Proceedings of the 6th International Conference on Strength of Metals and Alloys (ICSMA)*, Vol. 1, edited R.C. Gifkins (Pergamon, Oxford, 1982).
[27] P.M. Hazzledine, H.P. Karnthaler and E. Wintner, Phil. Mag. **32** 81 (1975).
[28] E. Nembach, Prog. Mater. Sci. **45** 275 (2000).
[29] R. Madec, B. Devincre and L.P. Kubin, Phys. Rev. Lett. **89** 255508-1 (2002).
[30] H. Neuhauser, in *Dislocations in Solids*, edited by F.R.N. Nabarro, Vol. 6 (North-Holland, Amsterdam, 1983).